Electron transport in nano-scaled piezoelectronic devices

Zhengping Jiang, Marcelo A. Kuroda, Yaohua Tan, Dennis M. Newns, Michael Povolotskyi et al.

Citation: Appl. Phys. Lett. **102**, 193501 (2013); doi: 10.1063/1.4804601
View online: http://dx.doi.org/10.1063/1.4804601
View Table of Contents: http://apl.aip.org/resource/1/APPLAB/v102/i19
Published by the American Institute of Physics.

Electron transport in nano-scaled piezoelectronic devices

Zhengping Jiang,[1] Marcelo A. Kuroda,[2] Yaohua Tan,[1] Dennis M. Newns,[2] Michael Povolotskyi,[1] Timothy B. Boykin,[3] Tillmann Kubis,[1] Gerhard Klimeck,[2] and Glenn J. Martyna[2]
[1]*Department of Electrical and Computer Engineering, Purdue University, West Lafayette, Indiana 47906, USA*
[2]*Physical Sciences, IBM TJ Watson Research Center, 1101 Kitchawan Rd., Yorktown Heights, New York 10520, USA*
[3]*Department of Electrical and Computer Engineering, The University of Alabama in Huntsville, Huntsville, Alabama 35899, USA*

(Received 7 April 2013; accepted 22 April 2013; published online 13 May 2013)

The Piezoelectronic Transistor (PET) has been proposed as a post-CMOS device for fast, low-power switching. In this device, the piezoresistive channel is metalized via the expansion of a relaxor piezoelectric element to turn the device on. The mixed-valence compound SmSe is a good choice of PET channel material because of its isostructural pressure-induced continuous metal insulator transition, which is well characterized in bulk single crystals. Prediction and optimization of the performance of a realistic, nano-scaled PET based on SmSe requires the understanding of quantum confinement, tunneling, and the effect of metal interface. In this work, a computationally efficient empirical tight binding (ETB) model is developed for SmSe to study quantum transport in these systems and the scaling limit of PET channel lengths. Modulation of the SmSe band gap under pressure is successfully captured by ETB, and ballistic conductance shows orders of magnitude change under hydrostatic strain, supporting operability of the PET device at nanoscale. [http://dx.doi.org/10.1063/1.4804601]

For decades, scaling of the Si-based MOSFET has enabled an exponentially increasing level of integration, packaging density, and clock speed. Today heat dissipation prevents any performance improvement through increasing clock frequency because the supply voltage has reached the scaling limit of MOSFET technology and cannot be lowered much below about 1 V without performance degradation. This fundamental power consumption issue has spurred the exploration of alternative switching mechanisms.[1]

The recently proposed Piezoelectronic Transistor (PET)[2,3] shows great potential to achieve a high ON/OFF ratio with a small voltage swing. In the PET, the limitation on the Subthreshold Swing (SS) imposed by the thermal tail of Boltzmann distribution is overcome through internal transduction. A small gate voltage (V_g) is transduced to an acoustic wave through a high-performance piezoelectric (PE) actuator fabricated from a relaxor piezoelectric material. The expansion of the PE layer exerts pressure to a channel layer consisting of a piezoresistive (PR) material capable of undergoing a pressure-induced insulator to metal transition. Rare earth chalcogenide PR materials—such as SmSe and SmTe—can vary conductance by several orders of magnitude when subjected to modest pressure changes.[4,5] Such a conductance change is predicted to exceed the maximum conductance gain achievable in the MOSFET, which is $10 \times V_g/60\,\text{mV}$.

The promising qualities of SmSe as a channel material have been experimentally demonstrated in thin film[6] and bulk crystalline form.[7,8] When a PET is scaled down to nanometer size, quantum effects will dominate carrier dynamics and classical transport models assuming a continuous medium will eventually fail to predict device performance. Though the bulk properties of SmSe have been studied by density functional theory (DFT),[9] quantum transport at realistic dimensions cannot be performed at the DFT level due to its prohibitive computational burden and inability to model non-equilibrium carrier transport. Approaches such as the empirical tight binding (ETB) method may open the possibility for the modeling of realistically extended devices provided that they can embody the physics underlying the piezoresistive effect. Indeed ETB has been widely used in simulations of nanoelectronic devices.[10–12]

In this work, the pressure induced Metal Insulator Transition in SmSe is modeled by ETB. The effect arises from the high sensitivity of the deformation potential to strain which rapidly shrinks the electronic bandgap. SmSe is parameterized for ETB[13] and results are calibrated to DFT calculations which in turn agree well with experimental measurements. Both ETB and DFT models capture the reported responses of the bandgap to external pressures.[8] The non-equilibrium Green's function (NEGF) method is then used to study ballistic transport with NEMO5.[14]

Our ETB parameterization features a basis transformation from DFT, in a plane wave representation, to an orthogonal TB basis—i.e., Löwdin orbitals[15]—and subsequent refinement by numerical optimization. With band structures and wavefunctions obtained from DFT calculations at the minimum-energy lattice constant, a DFT Hamiltonian is constructed and transformed to the TB Hamiltonian,[13] from which onsite energies and two center integrals for the TB basis are extracted following the Slater and Koster notation.[15,16] Effects of strain are accounted for through additional parameters which scale two center integrals and shift onsite energies according to bond stretching and bending.[10] Parameters are then refined with the simplex algorithm with fitting targets set to band structure along high symmetry directions $L \rightarrow \Gamma \rightarrow X$.[17] Finally, NEGF is employed to study the ballistic transport in SmSe with the new ETB parameters. Leads with the same modes as SmSe, perfectly coupled to

the channel, are assumed in transport, which is standard practice in quantum transport simulations.

The ETB model is determined based on the analysis of DFT results. First principles calculations within the generalized gradient approximation (GGA)[18] with spin-orbit (SO) coupling and a Hubbard-type on-site electron-electron repulsion U (Ref. 19) within the localized 4*f*-orbital are performed with the code ELK (http://elk.sourceforge.net/). An empirical value of U (U = 5.5 eV) is used to match x-ray photoemission spectra.[9] Figure 1(d) shows the DFT band structure (dashed lines). The double arrow indicates the large (~6 eV) splitting between the 6 occupied $4f_{5/2}$ bands and the 8 empty $4f_{7/2}$ bands, which arises partly from the Hubbard U and partly from the much smaller spin-orbit coupling. Figure 1(a) shows the decomposition of the DFT DOS in terms of the atomic species. The dominant weight of Sm projected DOS (pDOS) in the conduction band and Se pDOS in the lower bands implies an ionically bonded crystal with relatively weak covalent nearest neighbor interactions. This physics implies the need to include longer range orbital-orbital interactions in order to capture the valence and conduction bands. A decomposition of the DOS into angular momentum components in Figs. 1(b) and 1(c) shows that the valence band is primarily formed by Sm *4f* states (weakly coupled via Se *4p* states) and the conduction band is Sm *5d*. As a result, an ETB model with second nearest neighbor coupling is implemented with full sets of *spdfs** orbitals. SO couplings for *p*, *d*, and *f* orbitals are also included for both atoms given the high band splitting at critical symmetry points. Such coupling leads to an enhanced SO interaction within the *4f* manifold in order to capture the large $4f_{5/2}$-$4f_{7/2}$ splitting.

In the energy range relevant to transport, the band dispersion is accurately reproduced as shown in Fig. 1(d). The conduction band minimum and effective mass are primarily determined by the second nearest neighbor Sm-Sm coupling of the *5d* orbital. The matrix element ratios between *d* states ($V_{dd\sigma}$:$V_{dd\pi}$:$V_{dd\delta}$) are close to Harrison's model for transition elements.[20] The 4*f* band splitting, which stems from the Hubbard-type U and SO coupling, emerges in our model via an enhanced 4*f* band SO coupling.[21] Though the two splitting mechanisms are different, the appropriate symmetry is preserved. An optimized value of SO coupling $\delta_f = 2.06$ eV is obtained for Sm following the definition of Podolskiy and Vogl.[22]

The insulator to metal transition in SmSe originates from the reduction of the $4f_{5/2}$-*5d* bandgap under pressure until the occupied $4f_{5/2}$ eventually merges with the empty *5d*. Figure 2(a) shows the extracted indirect bandgap under two kinds of applied strain, hydrostatic pressure and uniaxial strain along the (100) direction. The TB parameters are fitted to the bandstructure under hydrostatic strain. The good match obtained for uniaxial strain without modification of the parameters confirms parameter transferability. Figures 2(b) and 2(c) plot the bandstructure for −3% hydrostatic and uniaxial strain, respectively. The dashed lines show the band edges when there is no strain applied. It is clearly seen that under strain, the conduction band will be broadened and the bandgap reduced towards zero. Hence the material continuously changes from insulating to metallic, at first because of thermal promotion of electrons from the filled $4f_{5/2}$ to the high-mobility 5d band and eventually because of the merging of these bands.

Figure 3(a) depicts the simulation structure and supercell for transport simulation. Figure 3(b) shows the complex band structure calculated at Γ with 0% and −3% hydrostatic strains. At zero bias condition, the equilibrium Fermi level positions are calculated self-consistently for strains from 0% to −3%. The calculated Fermi level positions are fixed as a boundary condition in the following simulations as labeled in Fig. 3(c).

Current is calculated when 0.05 V bias is applied to the drain contact which is assumed to drop linearly along a 6 nm SmSe channel (Fig. 3(a)) via integration over the whole Brillouin zone with *k*-space spacing of $0.1\pi/a$ ($a = 0.62$ nm). Figure 3(c) shows the transmission coefficient at Γ before and after applying bias. At zero bias, each transmission step corresponds to a sub-band in Fig. 3(b).[12] When a linear drop potential is applied, the values of transmission will not equal the numbers of incident waves and the localized bands will

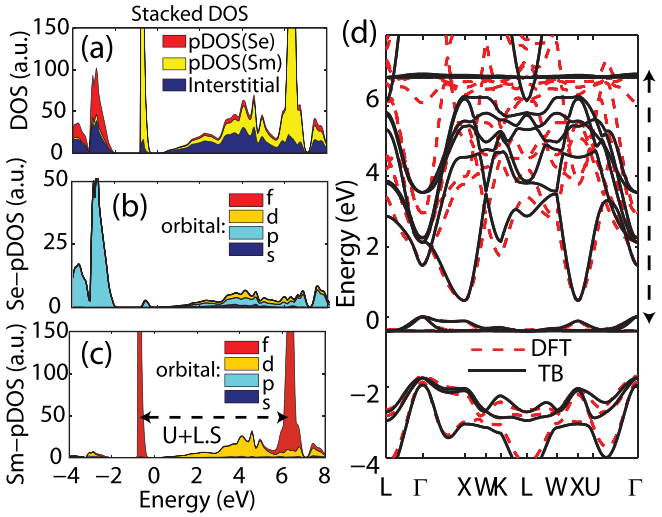

FIG. 1. Stacked DFT DOS and DFT/TB bandstructure comparison. (a) DOS within muffin-tin radius of Sm/Se and interstitial DOS. (b) DOS within Se atom decomposed by angular momentum. (c) DOS within Sm atom decomposed by angular momentum. (d) Band structure by spdfs*_SO TB model without strain (black) and DFT band structure without strain (red). E = 0 at top of valence band.

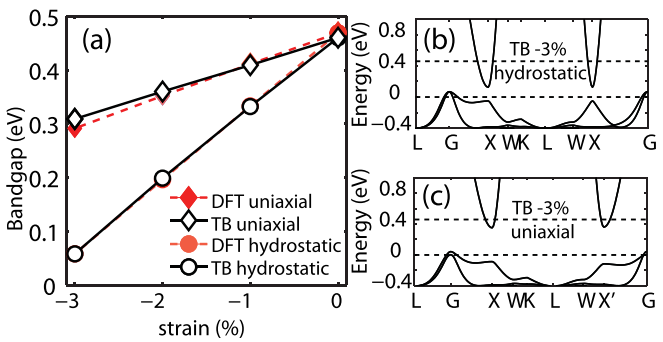

FIG. 2. Comparison of bandgap modulations with strain calculated by DFT and TB. (a) Bandgap extracted from DFT and TB bandstructure under hydrostatic and uniaxial strain. (b) TB bandstructure with $\varepsilon = -3\%$ compressive hydrostatic strain ($a_x = a_y = a_z = (1+\varepsilon) \times a_0$). (c) TB bandstructure with $\varepsilon = -3\%$ compressive uniaxial strain in growth direction ($a_x = (1+\varepsilon) \times a_0$; $a_y = a_z = a_0$). Dashed lines show bulk band edges in (b, c).

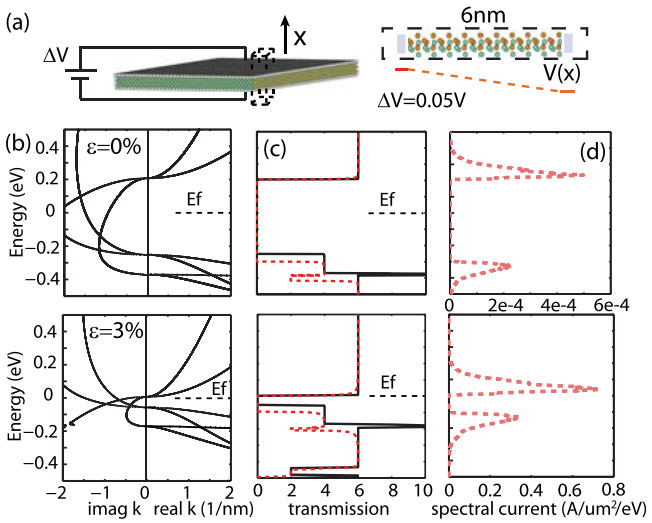

FIG. 3. Transport simulation for SmSe with hydrostatic strain. (a) Simulated structure in and 6 nm channel super cell in transport simulation. (b) Real and imaginary band structure for 0% and −3% hydrostatic strain. (c) Transmission with 0 V and 0.05 V linear drop potential. (d) Vd = 0.05 V, spectral current, dJ/dE, with linear drop potential.

no longer carry current due to the small band width. For example, comparing the dashed and solid lines in Fig. 3(c), the transmission diminishes at the top of the valence band and the transmission peak at E = −0.4 eV becomes a valley. Figure 3(d) plots the spectral current, dJ/dE, under the two strain conditions.[12,23] The large variation in the spectral current with strain ($>10^3$) indicates that a large piezoresistive effect is still observed in the ballistic regime. After the same calculations for 0% to −3% strain, ballistic resistances can be extracted. Ignoring the interference effects between real contacts and channel, a change of resistance by 3 orders of magnitude is obtained between −3% and 0% hydrostatic strain samples ($0.075\ \mathrm{A}/\mu\mathrm{m}^2$ and $4.58\times10^{-5}\mathrm{A}/\mu\mathrm{m}^2$). The exact value of the current requires accounting for the effect of the electrodes, which we will leave for future studies.

The transport results in SmSe presented here are based on the band structure as obtained from DFT calculations. At this level of sophistication, the predicted band width of the 4*f* valence band is of the order of 0.5 eV. As a result, the top of the 4*f* valence bands has relatively low hole masses allowing for the contributions to tunneling from modes in the valence band. In contrast, a much narrower width (of <50 meV), suggesting strong localization of the 4*f* states in SmX materials (X = S, Se, Te), can be deduced from data at low temperatures.[24–26] Such localization (due to strong correlations which are not properly be captured by DFT) would suppress tunneling via the valence band with the increase of hole masses. Further experimental investigation is required to properly characterize these material systems.

In this work, an ETB model accounting for second nearest neighbor coupling with full sets of *spdfs** orbitals has been developed to describe the band structure of rare-earth chalcogenide SmSe. The parameterization captures the band structure obtained from DFT and the effect of strain as obtained in DFT calculations. Calculations of the ballistic current in nanoscale films within the NEGF formalism demonstrate that a large piezoresistive effect is still observed in the ballistic regime. This work enables the realistic modeling of piezoelectronic devices and serves as a valuable tool to optimize its performance.

This work was partially supported by IBM PhD fellowship and NSF PetaApps award.

[1]T. N. Theis and P. M. Solomon, Science **327**(5973), 1600–1601 (2010).
[2]D. M. Newns, B. G. Elmegreen, X. H. Liu, and G. J. Martyna, Adv. Mater. **24**(27), 3672–3677 (2012).
[3]D. Newns, B. Elmegreen, X. H. Liu, and G. Martyna, MRS Bull. **37**(11), 1071–1076 (2012).
[4]M. Imada, A. Fujimori, and Y. Tokura, Rev. Mod. Phys. **70**(4), 1039 (1998).
[5]N. Mott, Rev. Mod. Phys. **40**, 677–683 (1968).
[6]M. Copel, P. M. Solomon, and T. M. Shaw (private communication).
[7]A. Jayaraman, A. K. Singh, A. Chatterjee, and S. U. Devi, Phys. Rev. B **9**(6), 2513–2520 (1974).
[8]A. Jayaraman, V. Narayanamurti, E. Bucher, and R. G. Maines, Phys. Rev. Lett. **25**(20), 1430–1433 (1970).
[9]V. N. Antonov, B. N. Harmon, and A. N. Yaresko, Phys. Rev. B **66**(16), 165208 (2002).
[10]T. B. Boykin, G. Klimeck, R. C. Bowen, and F. Oyafuso, Phys. Rev. B **66**(12), 125207 (2002).
[11]T. B. Boykin, G. Klimeck, and F. Oyafuso, Phys. Rev. B **69**(11), 115201 (2004).
[12]M. Luisier, A. Schenk, W. Fichtner, and G. Klimeck, Phys. Rev. B **74**(20), 205323 (2006).
[13]Y. Tan, M. Povolotskyi, T. Kubis, Y. He, Z. Jiang, G. Klimeck, and T. B. Boykin, J. Comp. Electron. **12**(1), 56–60 (2013).
[14]S. Steiger, M. Povolotskyi, H.-H. Park, T. Kubis, and G. Klimeck, IEEE Trans. Nanotechnol. **10**(6), 1464–1474 (2011).
[15]J. C. Slater and G. Koster, Phys. Rev. **94**(6), 1498 (1954).
[16]P. O. Löwdin, J. Chem. Phys. **18**, 365 (1950).
[17]See supplementary material at http://dx.doi.org/10.1063/1.4804601 for list of ETB parameters of SmSe.
[18]Y. Zhang and W. Yang, Phys. Rev. Lett. **80**(4), 890 (1998).
[19]V. I. Anisimov, J. Zaanen, and O. K. Andersen, Phys. Rev. B **44**(3), 943–954 (1991).
[20]W. A. Harrison and S. Froyen, Phys. Rev. B **21**(8), 3214–3221 (1980).
[21]M. D. Jones and R. C. Albers, Phys. Rev. B **79**(4), 045107 (2009).
[22]A. V. Podolskiy and P. Vogl, Phys. Rev. B **69**(23), 233101 (2004).
[23]Y. Meir and N. S. Wingreen, Phys. Rev. Lett. **68**(16), 2512–2515 (1992).
[24]M. B. Maple and D. Wohlleben, Phys Rev. Lett. **27**(8), 511–515 (1971).
[25]S. D. Bader, N. E. Phillips, and D. B. McWhan, Phys. Rev. B **7**(10), 4686–4688 (1973).
[26]C. M. Varma, Rev. Mod. Phys. **48**(2), 219–238 (1976).